

<https://www.overleaf.com/project/5bcc62e06844f52d76302aa2>

Laser beam steering using liquid crystals

Enes Lievens, Nathan Sennesael, Roeland Van Haecke

1. Introduction

1.1. Concept of liquid crystals

A liquid crystal (LC) is a liquid state of matter but which has similar properties to that of a crystalline solid in the sense that the molecules which make up the liquid show a certain degree of order in orientation. The molecules that make up the liquid crystal (called directors) are organic chains with a high degree of anisotropy, which is exactly what causes this spontaneous order. The rod-shaped molecules maximize their interface area as a result of Van der Waals interaction, minimizing the total energy of the system. A minimal energy corresponds to perfect alignment of the molecules, however, statistically there will be a deviation from this alignment due to the thermal energy of the molecules. This intrinsic disorder increases with the temperature of the LC, this is displayed in figure 1.

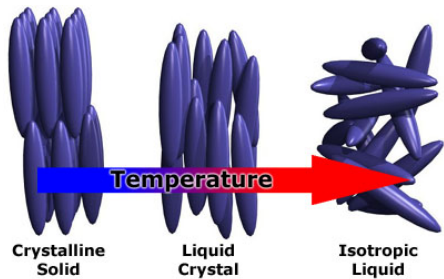


Figure 1: Concept liquid crystal. Image taken from [1]

When an external electric field is applied to the liquid crystal, a dipole is induced along the molecules. This results in a torque on the molecules of which the strength depends on the orientation of the director relative to the direction of the field. This allows us to manipulate the internal orientation of the crystal. This is displayed in figure 2.

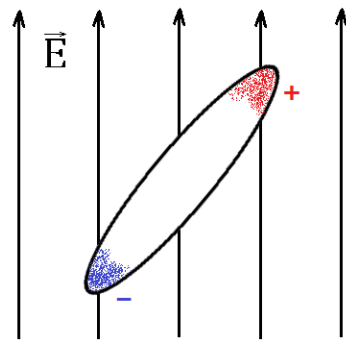


Figure 2: dipool

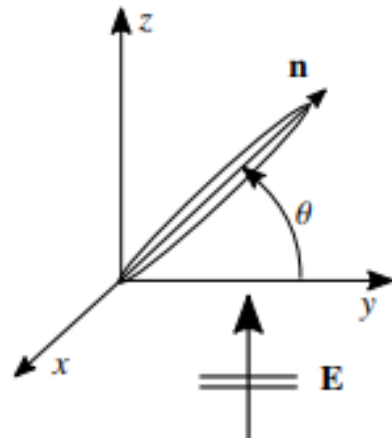


Figure 3: Orientation of the directors with the incident electric field.

This concept lays the foundation for numerous applications of liquid crystals. The objective of the research discussed in this paper is to redirect laser beams by making use of these anisotropic properties.

This anisotropy gives rise to a refractive index which depends on the orientation of the directors relative to

the electric field of the incident laser beam. Consider a wave traveling along the z -axis which is polarized along the y -axis, see figure 3. This wave impinges on a homogeneous liquid crystal, that is the average orientation of the directors is the same throughout the liquid crystal. In this application the directors will be oriented such that they lie in the polarization plane. Then the refractive index depends on the tilt angle θ and will be maximal resp. minimal for θ equal to 0 resp. $\pi/2$. This is due to the higher polarizability of the director when aligned along the electric field.

Since the orientation of the directors can be controlled by applying a voltage, a spatially varying refractive index profile can be created. To deflect a laser beam without causing divergence, a linear profile is required. To achieve this a theoretical model will be used to predict how this profile can be obtained by adjusting the physical parameters that characterize the problem.

2. Theoretical Model

2.1. 1D simulation

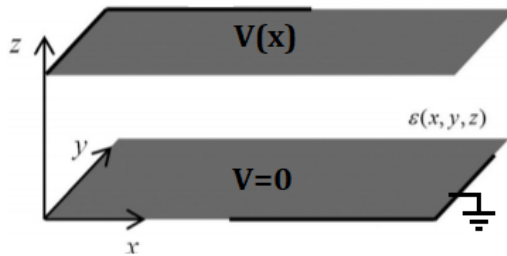


Figure 4: Geometry of the liquid crystal with bottom and top plate and electrodes. Image taken from [2]

The theoretical model is taken from [2]. It is presented here for the sake of completeness and is extended for multiple frequencies. This model is one dimensional, in the next section a simplified 2D model will be presented. Consider the geometry depicted in figure 4. A liquid crystal of length L is placed between a top layer at $z = d$ and a bottom layer at $z = 0$. The structure is assumed to extend infinitely in the y -direction. The top layer has a thickness d_1 and a conductivity σ . The bottom layer is assumed to be perfectly electric conducting and is grounded. The permittivity of the liquid crystal is anisotropic and therefore has to be described by a 3×3 tensor. Let \mathbf{n} be the statistical average of the orientation unit vectors of the directors, then the permittivity is given by:

$$(\bar{\varepsilon})_{ij} = \varepsilon_{\perp} \delta_{ij} + \Delta \varepsilon n_i n_j \quad \Delta \varepsilon = \varepsilon_{\parallel} - \varepsilon_{\perp} \quad (1)$$

Note that the permittivity is also frequency dependent. In this paper only two frequency ranges will matter, the frequency of the applied voltage to change the direction of the directors and the frequency of the laser beam that travels through the LC. The theory that we described earlier indicates that a DC voltage would be optimal. However, this would cause free ions in the LC to accumulate on the electrodes. Instead, a low frequency AC voltage is used which can range from 100 kHz up to a few hundred kHz.

As long as the thickness d of the LC is much smaller than the length L , the problem can be treated one dimensionally. The fields and material properties are only a function of the x -coordinate and the applied electric field is assumed to be approximately parallel to the z -axis. Of course, microscopically this is not correct since the positioning of the molecules varies with z -values as depicted in figure 5. To take this into account the relevant quantities can be averaged out in the z -direction.

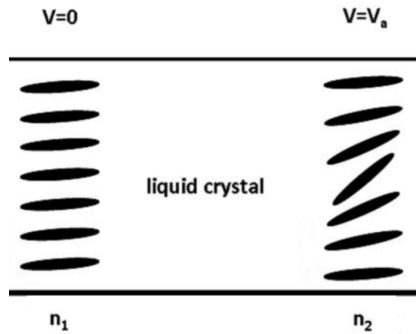


Figure 5: Microscopic view

The x - and y -component of the electric field can be neglected in this approximation. Gauss's law is:

$$\nabla \cdot \mathbf{D} = \rho_f \quad (2)$$

Combining (1) with (2), taking into account that $\mathbf{n} = \cos(\theta)\mathbf{u}_y + \sin(\theta)\mathbf{u}_z$ and that there is no free space charge in the LC shows that D_z is in good approximation z -independent:

$$D_z(x) = \varepsilon_{zz}(x, z) E_z(x, z) \quad (3)$$

Since the frequencies driving the LC are sufficiently low a scalar potential V can be defined. This allows to define an effective permittivity as follows:

$$D_z(x) = -\varepsilon_{eff}(x) \frac{V(x)}{d} \quad (4)$$

The scalar potential is given by:

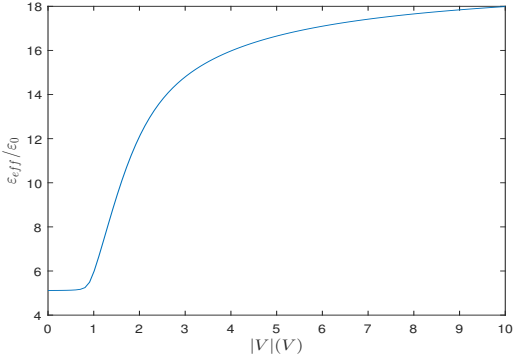


Figure 6: Effective permittivity of the LC as a function of the root-mean-square applied voltage for the liquid crystal E7.

$$V(x) = - \int_0^d E_z(x, z) dz. \quad (5)$$

This results in:

$$\frac{1}{\varepsilon_{eff}(x)} = \frac{1}{d} \int_0^d \frac{1}{\varepsilon_{zz}(x, z)} dz. \quad (6)$$

The orientation of the directors is obtained by minimizing the total free energy of the liquid crystal. The full details will not be given in this section. In the next section such details are presented for the 2D case. For more information the reader is referred to [3]. The results for the liquid crystal E7 are shown in figure 6. It is important to note that the directors react to the root-mean-square (RMS) value of the electric field and not its amplitude.

This effective permittivity can be used to set up a simplified differential equation that can be solved numerically. The top plate, which has low conductivity, carries a surface current \mathbf{K} . The expression for this current is given by the following equation:

$$\mathbf{K} = -\sigma d_1 \frac{dV}{dx} \mathbf{u}_x. \quad (7)$$

Conservation of charge results in:

$$\frac{dK}{dx} + j\omega\rho_s = 0. \quad (8)$$

Here ρ_s is the surface charge at the weakly conducting layer-LC boundary and is obtained using the boundary condition for the dielectric displacement:

$$\rho_s = \varepsilon_{eff} \frac{V}{d} \quad (9)$$

Combining the above gives the final differential equation:

$$\frac{d^2V}{dx^2} = j \frac{\omega \varepsilon_{eff}}{d_1 d \sigma} V. \quad (10)$$

Remark that ε_{eff} depends on the RMS-value of the applied voltage, which in turn is position dependent. This non-linear differential equation together with the boundary conditions $V(-L/2) = V_1$ and $V(L/2) = V_2$ can be solved numerically in Matlab.

We define the characteristic length as:

$$x_0^c = \sqrt{\frac{\sigma d_1 d}{\omega \varepsilon_\perp}}. \quad (11)$$

Equation (10) can then be rewritten as:

$$\frac{d^2V}{dx^2}(x) = j \left(\frac{1}{x_0^c} \right)^{-2} \frac{\varepsilon_{eff} (|V(x)|/\sqrt{2})}{\varepsilon_\perp} V(x) \quad (12)$$

where all dependencies are explicitly written for clarity. The goal is to create a linearly varying refractive index profile. To achieve this the voltage profile must be tunable. One way to accomplish this is by introducing more parameters. When the LC is driven by two frequencies one obtains a coupled system of differential equations for the driving voltages V_1 and V_2 with frequencies ω_1 and ω_2 respectively. This gives:

$$\frac{d^2V_1}{dx^2} = j \frac{\omega_1 \varepsilon_{eff}}{d_1 d \sigma} V_1, \quad (13)$$

$$\frac{d^2V_2}{dx^2} = j \frac{\omega_2 \varepsilon_{eff}}{d_1 d \sigma} V_2, \quad (14)$$

where ε_{eff} is now a function of $\sqrt{(|V_1|^2 + |V_2|^2)/2}$. Once the voltage profile is calculated the refractive index can be obtained. As the LC is anisotropic its refractive index depends on its orientation. The refractive index when the polarization of the incident light is perpendicular to the axis of the director is called the ordinary refractive index and is denoted n_o . When the polarization of the incident light is parallel to the axis of the director the refractive index is called the extraordinary refractive index and is denoted n_e . Due to a higher polarizability along the axis $n_e > n_o$. For all angles θ between 0 and $\pi/2$ the effective refractive index is given by [2]:

$$n_{eff} = \frac{n_o n_e}{\sqrt{n_e^2 \sin^2(\theta) + n_o^2 \cos^2(\theta)}} \quad (15)$$

Once the refractive index profile is known the light intensity on a detection screen after the LC can be determined. To treat this problem one dimensionally an

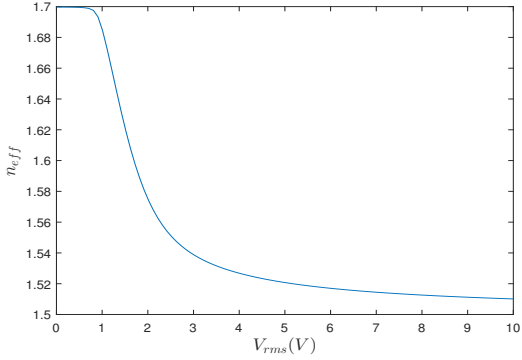


Figure 7: Effective refractive index of the LC as a function of the root-mean-square applied voltage for the liquid crystal E7 ($n_o = 1.5$ and $n_e = 1.7$).

average refractive index must be introduced. In order to do this consider the optical path length a ray traces from a point A at the front of the LC ($z = 0$) to a point B at the back of the LC ($z = d$).

$$OPL = \int_A^B n_{eff} ds. \quad (16)$$

Since the incoming ray is paraxial and the changes in n_{eff} are small this simplifies to:

$$OPL \approx \int_0^d n_{eff} dz. \quad (17)$$

An average refractive index can then be defined by stating that $OPL = n_{avg}d$, such that:

$$n_{avg} = \frac{1}{d} \int_0^d n_{eff} dz. \quad (18)$$

The effective refractive index as a function of the RMS-voltage for a one dimensional cell is shown in Figure 7. As can be seen from this figure the refractive index starts changing from an offset RMS-value of about 1V. In the range 1V – 2V it is approximately linear. Thus in this range it will be possible to achieve a linearly varying refractive index along the LC cell if the potential distribution also varies linearly. However, when higher beam steering angels have to be achieved a nonlinear potential distribution will be necessary. To account for the full vectorial nature of light would make the problem unnecessarily complicated. Since the dimensions of the LC are much larger than the wavelength and variations in the refractive index occur over length scales much larger than the wavelength scalar wave theory can be used. Consider the setup depicted in Figure 8. The liquid crystal is placed at the left side

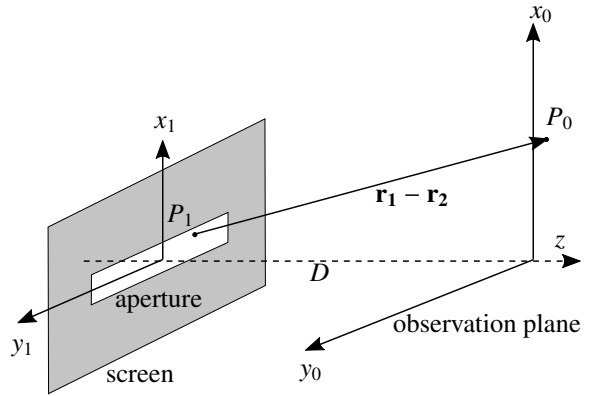


Figure 8: Geometry considered in Fraunhofer approximation.

of the screen. The back of the LC (where the light will be emitted) is represented by the aperture, which is located at $z = 0$ for convenience. Given the amplitude $U(x_1, y_1)$ of the scalar wave function at the aperture the amplitude $U(x_0, y_0)$ at a point P_0 on the detection screen can be determined. When D is large the result is given by the far field limit of the Fresnel diffraction formula (Fraunhofer approximation) [4]:

$$U(x_0, y_0) = \frac{-e^{-jkd}}{j\lambda D} e^{-\frac{jk}{2D}[x_0^2 + y_0^2]} \int_A U(x_1, y_1) e^{j\frac{2\pi}{\lambda D}[x_0 x_1 + y_0 y_1]} dS, \quad (19)$$

where the integration extends over the aperture. The incident light is a Gaussian beam. For the dimensions of the LC considered here the Rayleigh range is much larger than the thickness of the LC such that the incident amplitude U_i around $z = -d$ is approximately given by:

$$U_i(r, z) = U_0 \exp\left(-\frac{r^2}{w_0^2}\right) \exp(-j kz) \quad (20)$$

where w_0 is the beam waist of the incident beam at the front of the LC and r the radial distance measured from the axis of the beam. The LC introduces a phase retardation such that when d is sufficiently small the amplitude at the aperture is given by (neglecting any reflection or absorption losses):

$$U(x_1, y_1) = U_0 \exp\left(-\frac{x_1^2 + y_1^2}{w_0^2}\right) \exp(-jk(n_{avg}(x_1) - 1)d). \quad (21)$$

Since the amplitude falls off sufficiently fast the integration in the y -direction can be taken to cover the entire y -axis such that this integration can be done analytically:

$$U(x_0, y_0) = j \sqrt{\pi} \frac{U_0 w_0}{\lambda D} e^{-jkD} e^{-\frac{jk}{2D}[x_0^2 + y_0^2]} e^{-(\frac{\pi w_0 y_0}{\lambda D})^2} \int e^{-\frac{x_1^2}{w_0^2}} e^{-jk(n_{avg}(x_1)-1)d} e^{\frac{2\pi}{\lambda D_0} x_1} dx_1. \quad (22)$$

It is clear that a linear varying refractive index results in an exiting beam which remains Gaussian and thus has a minimal angular spread. Any deviations from such a linear profile result in a larger angular spread which can be quantified using expression (22).

2.2. Cross section simulation

The previous model has the advantage that it is one dimensional and thus requires less computational time to solve. However, when the thickness of the cell d is no longer much smaller than the length of the cell L the previous model becomes less accurate. Such a configuration is desirable because it allows for larger beam steering angles. The lower accuracy is mainly because only the z -component of the dielectric displacement \mathbf{D} is considered. Furthermore D_z is assumed to be constant along the z -direction and the z -dependent permittivity is replaced by an effective permittivity, eliminating all z -dependencies. Another important difference is that the alignment of the directors at the top and bottom layer now plays a role. If the directors lie parallel to the electrodes they will tend to twist, they will align with the x -component of the electric field. When the directors lie perpendicular to the electrodes the x -component of the electric field only results in tilt. To estimate the accuracy of the 1D model a simulation of the cross section of the cell is also carried out. In order not to unnecessarily complicate things it is assumed the directors lie perpendicular to the electrodes. In this a way only two fields have to be calculated: the potential $V(x, z)$ and the tilt angle $\theta(x, z)$. The potential is simply governed by Gauss's law:

$$-\nabla \cdot (\bar{\epsilon} \nabla V) = 0 \quad (23)$$

where $\bar{\epsilon}$ is given by Equation (1) and $\mathbf{n} = \cos(\theta)\mathbf{u}_x + \sin(\theta)\mathbf{u}_z$. The equation governing the twist is obtained by minimizing the free energy of the liquid crystal. This energy consists of two contributions. First the elastic energy is due to the deformation of the liquid crystal. Second the electrostatic energy is due to alignment of

dipoles with an applied electric field. The total free energy density of a nonpolar, nonenantiomorphic (no chiral molecules with different mirror images present) liquid crystal where bend, splay and twist elastic constants are equal (one constant approximation) is given by [3]:

$$g = \frac{1}{2} K [(\nabla \cdot \mathbf{n})^2 + (\nabla \times \mathbf{n})^2] - \frac{1}{2} [\epsilon_\perp \mathbf{E}^2 + \Delta \epsilon (\mathbf{n} \cdot \mathbf{E})^2]. \quad (24)$$

The one constant approximation greatly simplifies the equations. Here K is taken to be the average of the splay and bend constants since no twist is present. The free energy $\int g dV$ is minimized using the Euler-Lagrange equation. This results in an equation for the tilt angle:

$$-K \nabla^2 \theta = \frac{1}{2} \Delta \epsilon (-\sin(2\theta) E_x^2 + \cos(2\theta) E_x E_z + \sin(2\theta) E_z^2). \quad (25)$$

Here \mathbf{E} is the root-mean-square value of the sinusoidally varying electric field. The problem is made dimensionless by setting $x' = x/L$ and is solved on the domain shown in Figure 9.

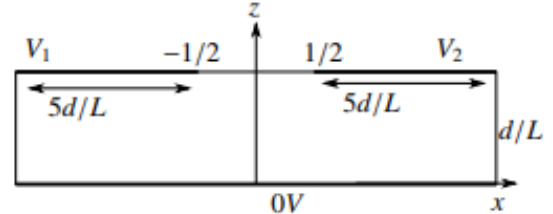


Figure 9: Computational domain for cross section simulation. The electrodes are held at voltages V_1 and V_2 .

The top left and right electrodes are kept at voltages V_1 and V_2 respectively. The weakly conducting layer between the electrodes is supposed to be thick enough such that the characteristic distance in this case is much larger than the electrode gap. This allows to impose a linearly varying potential between the electrodes (Matlab does not allow boundary conditions different from Dirichlet or generalized Neumann conditions which is necessary for thin weakly conducting layers). The conducting layer at the bottom is grounded. The pretilt of the director at the bottom and top layer is 2° . The electrodes are made sufficiently long such that at the boundaries at the side the potential and tilt angle do not vary much such that there the boundary condition becomes

$\partial V/\partial n = 0$ and $\partial \theta/\partial n = 0$. The Equations (23) and (25) form a system of nonlinear partial differential equations and can be solved numerically using Matlab.

3. Methods

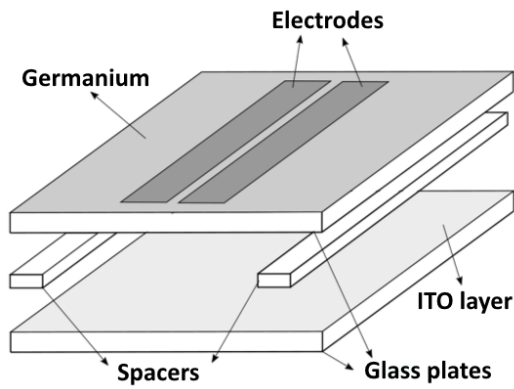


Figure 10: components of the beam steering device

3.1. Material selection and production

In order to deflect a laser beam, the LC has to have similar effects as a prism, this means that a linear variation in the phase front is induced as the laser beam transmits through the LC. This can be achieved by applying an electrical potential distribution across the LC which causes a linearly varying refractive index. This electrical potential is theoretically determined through the theoretical model described in the previous section.

In order to achieve such a potential distribution a weakly conductive material is added between two aluminum electrodes. In this project amorphous germanium is used as a weak conductor due to its suitable properties and high sheet resistance. The germanium is coated on top of the substrate using a technique called sputtering in which germanium is bombarded with high energy electrons and evaporated onto the substrate.

The liquid crystal E7 was used, which is a mixture of cyanobiphenyls with long aliphatic tails, an example chemical structure is displayed in Figure 11.

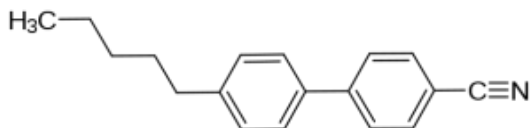


Figure 11: chemical structure [2].

The interface where the LC is confined by the glass plates is also spin coated with nylon. A nylon solution is applied to the glass plates which are then rotated at several hundreds to even thousands of RPM, this way the thickness of the coating can also be tuned. Nylon molecules are long synthetic polymer chains. This coating is then gently rubbed in one direction to align the nylon chains. When the LC is applied to the glass plates, the directors at the surface of the glass will align with the nylon chains, setting a foundation for the orientation of the other directors in the LC. The direction of the rubbing can either be chosen to be parallel or perpendicular to the electrodes. When the alignment is chosen to be perpendicular to the electrodes, the one dimensional approximation is debilitated. When the alignment is chosen parallel to the electrodes, we have to take into account that they may also twist towards the electrodes where the voltages are applied, since there is a potential difference on the upper plate.

On the bottom plate an ITO (Indium Tin Oxide) coating is applied, which is a transparent conductor, this is required to approximate the perfect electrically conducting grounding as is used in the theoretical simulation.

The spacer which determine the thickness of the device are of the order of several micrometers. The ideal orders of magnitude are determined through the theoretical model.

3.2. Optical setup

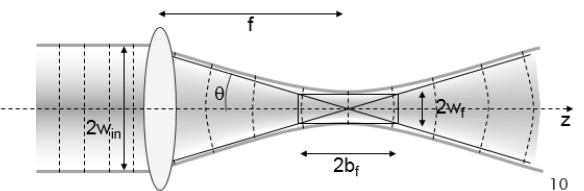


Figure 12: Focusing a Gaussian beam

Because of the small dimensions of a LC a system of lenses is used to focus the beam between the electrodes of the LC. In order to avoid diffraction, a Gaussian beam has to be narrowed to be smaller than the gap between the electrodes. The laser used in the project is a Helium-Neon laser with a wavelength of 632.8 nm. This laser has a beam diameter of approximately 1 mm and has to be focused to a beam diameter of below 60 μm to fit in between electrodes spaced 80 μm apart. If the outgoing beam converges with a small enough angle θ the following approximation can be made:

$$\tan(\theta) \approx \theta = \frac{w_{in}}{f} \quad (26)$$

θ is also related to the beam width w_f in the focal plane:

$$\theta = \frac{\lambda}{\pi w_f} \quad (27)$$

And therefore:

$$f = \frac{\pi w_f w_{in}}{\lambda} \quad (28)$$

substituting in $w_f \leq 60 \mu\text{m}$, $w_{in} = 0.5 \text{ mm}$ and $\lambda = 632.8 \text{ nm}$ gives us a focal length of $f \leq 0.1489 \text{ m}$ or $f_{max} \approx 15 \text{ cm}$. This beam only stays focused within the Rayleigh range, therefore this range has to be large enough so that it is greater than or the thickness of the LC ($\approx 20 \mu\text{m}$):

$$b_f = \frac{\pi w_f^2}{\lambda} = 4.468 \text{ mm} \quad (29)$$

Of course, lenses with a smaller focal length could be used as they result in a smaller focal width, but the downside to these lenses are that they expand faster after they pass their focal point, which makes it less suitable for beam steering applications. So a lens with $f = f_{max}$ will result in the best beam steering.

3.3. Microscopy analysis

The change in refractive index of the liquid crystal can be seen using a microscope and two parallel polarizers, this is because the liquid crystal is a birefringent medium. The setup is shown in figure 13. The linearly polarized light after the first polarizer has the following form [3]:

$$\vec{E}_{in} = \begin{pmatrix} E_x \\ E_y \end{pmatrix} = \begin{pmatrix} E_0 \cos(\alpha) \\ E_0 \sin(\alpha) \end{pmatrix} \quad (30)$$

After passing through the sample the light becomes elliptically polarized:

$$\vec{E}_{LC}(z) = \begin{pmatrix} E_x \exp(ik_e z) \\ E_y \exp(ik_o z) \end{pmatrix} \quad (31)$$

Because of this the ray of light has a component that can pass through the polarizer. Using the Jones calculus for the optical polarizer we get:

$$\begin{aligned} \vec{E}_{out} &= \hat{A} \vec{E}_{LC}(z = d) \\ &= \begin{pmatrix} \sin^2(\alpha) & -\cos(\alpha) \sin(\alpha) \\ -\cos(\alpha) \sin(\alpha) & \cos^2(\alpha) \end{pmatrix} \begin{pmatrix} E_x \exp(ik_e d) \\ E_y \exp(ik_o d) \end{pmatrix} \end{aligned} \quad (32)$$

This simplifies to the output light field and light intensity behind the analyzer: (with d the thickness of the LC and k_o and k_e the wave numbers of the ordinary and extraordinary rays respectively)

$$\vec{E}_{out} = E_0 \sin(2\alpha) \sin\left(\frac{\Delta kd}{2}\right) \exp\left(\frac{i(k_o + k_e)d}{2}\right) \begin{pmatrix} \sin\alpha \\ \cos\alpha \end{pmatrix} \quad (33)$$

$$|\vec{E}_{out}|^2 = E_0^2 \sin^2(2\alpha) \sin^2\left(\frac{\Delta kd}{2}\right) \quad (34)$$

or:

$$T = T_0 \sin^2(2\alpha) \sin^2\left(\frac{\Delta kd}{2}\right) \quad (35)$$

$$\Rightarrow I = \sin^2(2\alpha) \sin^2\left(\frac{\Delta kd}{2}\right) \quad (36)$$

For a maximum intensity the LC gets lined up so that $\alpha = 45^\circ$. Together with $\Delta k = \frac{2\pi\Delta}{\lambda}$ it gives the final equation:

$$I = \sin^2\left(\frac{\pi\Delta nd}{\lambda}\right) \quad (37)$$

with $\Delta n = n_e(x) - n_0$. In the case of a beam steering LC device the refractive index $n_e(x)$ needs to be linear, in the ideal case this means:

$$n_e(x) = n_0 + Cx \Rightarrow I \propto \sin^2\left(\frac{C\pi d}{\lambda}x\right) \quad (38)$$

With C a constant that determines the slope of the refractive index.

From this it is now clear that when looking at the LC through a microscope the refractive index will be perfectly linear when the intensity pattern is a pattern of light and dark fringes as shown in Figure 14.

4. Results

4.1. 1D Theoretical results and optimization

Equation (10) is solved numerically in Matlab. The problem is made dimensionless by setting $x' = x/L$. The voltage distribution was calculated for several characteristic distances with boundary conditions $V(0) = 1.4V$ and $V(L) = 2.8V$ (amplitude values). The result is shown in Figure 15. The associated refractive index profiles are shown in Figure 16. For characteristic distances comparable or larger than L the index profile is approximately linear, whereas for $x_c < L$ the index profile is not.

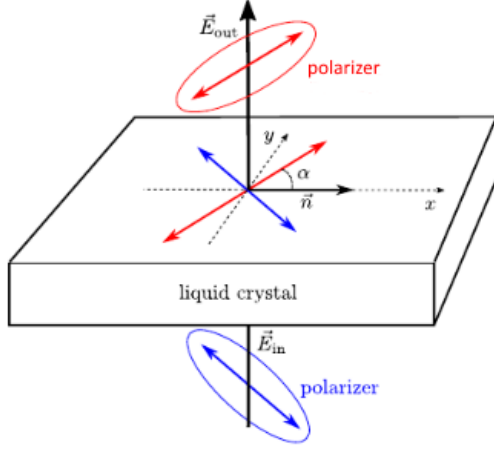


Figure 13: Light traveling through the liquid crystal will take one of two paths, ordinary or extraordinary, perpendicular or parallel to the director, depending on its polarization.

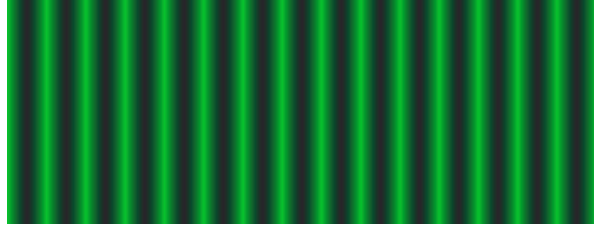


Figure 14: ideal intensity pattern for a linear refractive index

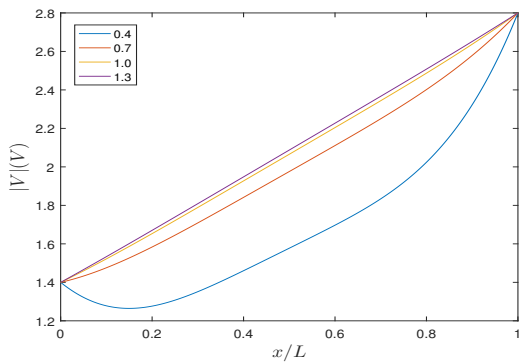


Figure 15: Voltage distribution for several characteristic distance (expressed as a fraction of L) for boundary conditions $V(0) = 1.4V$ and $V(L) = 2.8V$.

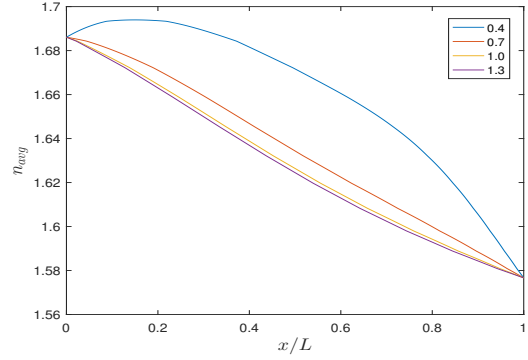


Figure 16: Refractive index profile for several characteristic distance (expressed as a fraction of L) for boundary conditions $V(0) = 1.4V$ and $V(L) = 2.8V$.

To achieve optimal beam steering for angles as large as possible the applied voltages and frequencies can be optimized. To increase the number of degrees of freedom different frequencies can be applied. From equations (14) it can be seen that this results in six parameters: the two boundary conditions for V_1 and V_2 and their characteristic distances, controlled by the frequency. To optimize the index profile these coupled equations were solved numerically in Matlab. The obtained index profile is than compared to a linear profile. The deviation from such a linear profile can be used as a cost function that has to be minimized. The cost c is calculated as the mean square deviation:

$$c = \frac{1}{L} \int_0^L (n_1 - \Delta n x - n(x))^2 dx. \quad (39)$$

Here $\Delta n = \theta L/d$ where θ is the deflection angle of the beam. n_1 is the desired refractive index at $x = 0$ which is taken as high as possible such that Δn can be as high as possible. Optimization was done in Matlab using the *fmincon* function. This function uses a gradient-based search algorithm. The optimal parameters were calculated for different angles. In a first step the optimal parameters were determined for a small angle of 0.5. The resulting parameters were then used as an initial guess for the next angle and so forth. The resulting values of the parameters are shown in Table 1. The values used were $n_1 = 1.68$ and $d/L = 1/4$. It is clear that the secondary voltage remains practically zero. This indicates multiple frequencies might not be able to improve beam steering quality. The linear index profiles for the calculated optimized parameters are shown in Figure 17. For angles larger than 2.0° the profile starts to deviate. Optimization yields no improvements.

Table 1: Optimized values of the parameters for $n_1 = 1.68$ and $d/L = 1/4$. (voltages in RMS values)

$\theta(deg)$	$V_1(0)(V)$	$V_1(L)(V)$	x_{c1}/L	$V_2(0)(V)$	$V_2(L)(V)$	x_{c2}/L
0.5	1.06	1.32	1.00	0.00	0.00	0.97
1.0	1.06	1.57	1.00	0.00	0.01	1.04
1.5	1.03	1.88	1.00	0.00	0.03	1.07
2.0	1.00	2.22	1.00	0.00	0.02	1.47
2.2	0.98	2.21	1.00	0.00	0.03	1.44

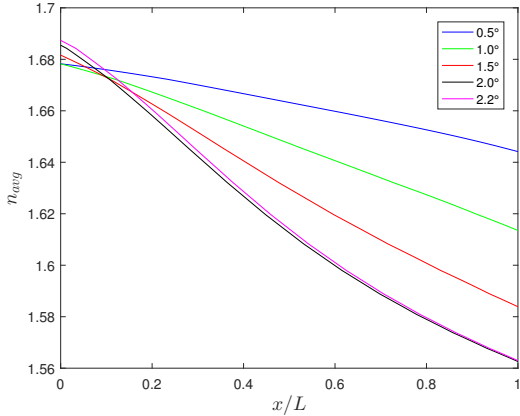


Figure 17: Refractive index profiles for optimized parameter values.

4.2. Cross section simulation

Equations (23) and (25) are solved numerically using the Matlab PDEToolbox. Because these partial differential equations are nonlinear they have to be solved iteratively. As an initial guess for the potential the permittivity is assumed constant resulting in the Laplace problem $\nabla^2 V = 0$ to be solved. This initial guess is then used to solve Equation (25). With the first guess of the tilt angle Equation (23) can now be solved. This process is repeated until convergence of the solution is obtained. The properties of the liquid crystal E7 are the following: $\Delta\epsilon = 14.5\epsilon_0$, $\epsilon_\perp = 5.1\epsilon_0$, $K_{11} = 12\text{ pN}$ and $K_{33} = 19.5\text{ pN}$. In the one constant approximation $K = 15.75\text{ pN}$ is used. To compare with the one dimensional model the 2D problem is solved for a number of cases. The left electrode is kept at 1.0 V while the right electrode varies from 1.5 V to 3.0 V in steps of 0.5 V (RMS-values). The ratio between d and L is 1/3. The 1D problem is solved for the same boundary conditions using $x_c = 5L$ such that the voltage profile is also linear like in the 2D case. To compare with the 1D case the average effective refractive index is calculated using Equations (15) and (18). The result is shown in Figure 18. At the left electrode the refractive index remains the same for the 1D case. While for the 2D case it lowers

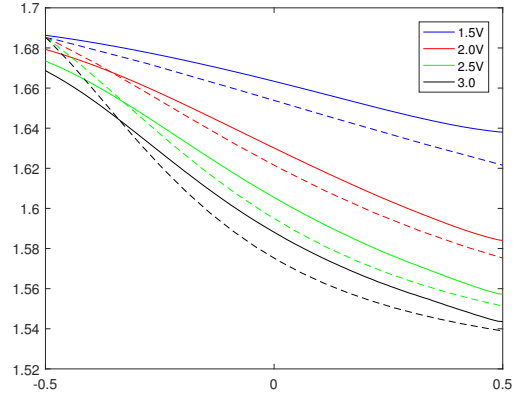


Figure 18: Comparison of 1D simulation (dashed line) and 2D simulation (full line) results for the average refractive index. The left electrode is kept at voltage of 1.0 V (RMS) while the voltage of the right electrode takes on the RMS-values 1.5 V (blue), 2.0 V (red), 2.5 V (green) and 3.0 V (black).

for increasing voltages at the right electrode. Furthermore it can be seen that globally the absolute value of the refractive index is higher for the 1D case. However qualitatively the 1D and 2D cases show a similar shape.

4.3. IV Characterization of the sample

Because the characteristic distance is a critical parameter a current measurement was conducted to check the resistivity of the germanium layer. From previous measurements the sheet resistance of a 5 nm thick germanium layer was found to be in the order of $10 \times 10^{10} \Omega/\text{sq}$. One problem that occurred when measuring the current through the germanium layer with a thickness of 5nm was that the current dropped after some time. This is because when sputtering a layer of only a few nanometers thick you can't be sure that the germanium layer is in good contact with the electrodes and due to some capacitive effects of the LC and electrical screening of the ions in the LC (a DC voltage is applied when measuring the current). This current drop is shown in figure 19. These effects can be minimized by increasing the thickness of the germanium layer, the

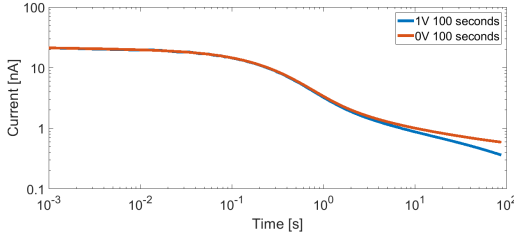


Figure 19: current plot of an IV measurement of a LC sample with a 50 nm Ge layer,a current drop occurs due to capacitive effects and ionic screening of the LC

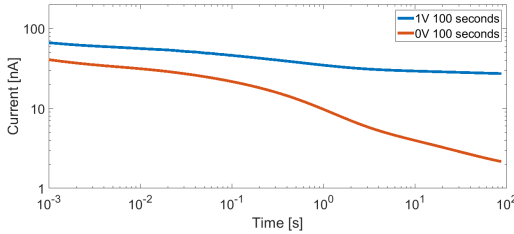


Figure 20: current plot of an IV measurement of a LC sample with a 50 nm Ge layer, the current remains almost constant through the entire measurement and the capacitive and screening effects are almost negligible

only downside being that this changes the characteristic distance. When for electrodes with a spacing of $100\ \mu\text{m}$, a germanium layer of 50 nm and a length on the order of 1 cm a voltage of 1 V is applied a current of 50 nA–100 nA is expected. A voltage of 1 V was applied for 100 s while measuring the current. Then the voltage was turned off and the current was measured for an additional 100 s. The resulting current as a function of elapsed time is shown in figure 20.

4.4. Polarization microscopy

As explained in section 3.3 Microscopy analysis, a setup as shown in Figure 13 can be used to determine the change in refractive index. In this paper however a full analysis and breakdown of the picture would take us too far and would require a single wavelength light source and a high quality camera to take these pictures. A single wavelength was not used here because of the thickness of the germanium layer, which only let through a small fraction of the incident light (the microscope used only produced white light and placing a monochromatic filter after the light source caused the light source to be too dim to see anything, thus the white light source had to be used). A short derivation will be given and the polarizer microscopy pictures will be used to check if the LC is working as predicted by

the theoretical model used in this paper.

Starting from equation 38 one can easily find an expression for the refractive index $n_e(x)$:

$$\Delta n = \frac{\lambda}{\pi d} \arcsin(\sqrt{I(x)}) \quad (40)$$

Or:

$$n_e(x) = n_0 + \frac{\lambda}{\pi d} \arcsin(\sqrt{I(x)}) \quad (41)$$

Now the only challenge is to analyze and process the image in order to find an expression for $I(x)$. This refractive index profile can be seen in 26 and is extracted from the intensity profile seen in figure 25. The intensity profile roughly resembles a \sin^2 function with decreasing period T , so in order to convert this to the refractive index profile, the intensity profile is split up in different sections with different periods, each quarter wave is approximated to be a perfect sine wave so that the following simplification can be made:

$$I(x) \propto \sin^2\left(\frac{2\pi}{T}x\right) \quad (42)$$

$$\Rightarrow n_e(x) = n_0 + \frac{\lambda}{\pi d} \frac{2\pi}{T} x \quad (43)$$

$$n_e(x) = n_0 + \frac{2\lambda}{Td} x \quad (44)$$

Which is linear as long as the period does not change, this gives rise to a piecewise linear approximation of the refractive index with an increasing slope for a decreasing period, which explains the refractive index profile in figure 26. Microscopy images for different voltages and frequencies are shown in figures 21 to 24.

5. Discussion

5.1. Theoretical results and optimization

The results shown in figure 15 can be explained by the frequency behavior of the cell and the weakly conducting layer. At high frequencies, thus small x_c , the LC acts as a capacitor. The current that is drawn from the electrodes passes partly through this capacitance resulting in a voltage drop. For low frequencies this effect is negligible and all current passes through the weakly conducting layer, resulting in a linear voltage profile. Because of the chosen voltage range the linear index profile in figure 16 is fairly linear for characteristic distances not too small. As can be seen from figure 7 in the RMS-voltage range 1V – 2V, the refractive index is approximately linear. For smaller x_c , due to the voltage

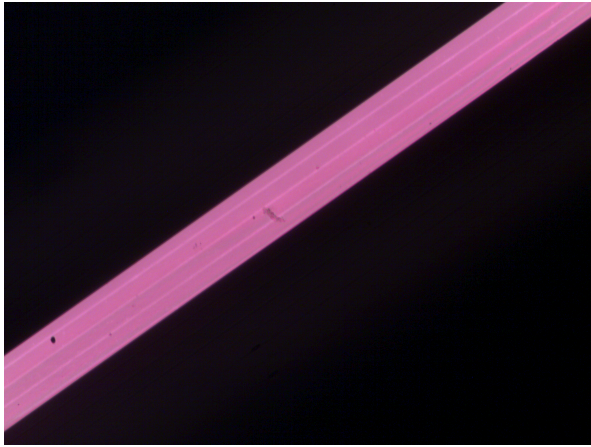


Figure 21: The LC through the polarizer microscope with an external voltage source of 2 V_{RMS} at a frequency of 200Hz

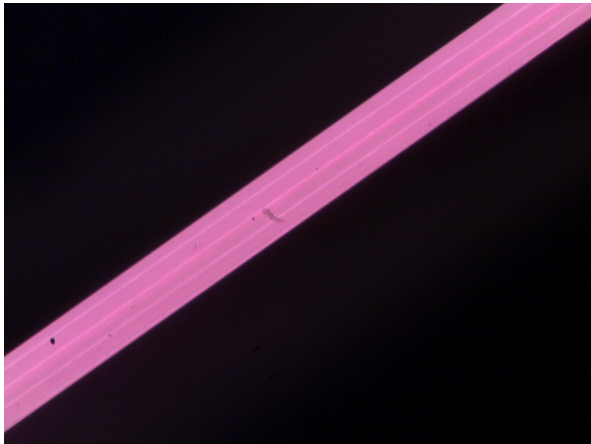


Figure 22: The LC through the polarizer microscope with an external voltage source of 2 V_{RMS} at a frequency of 20kHz

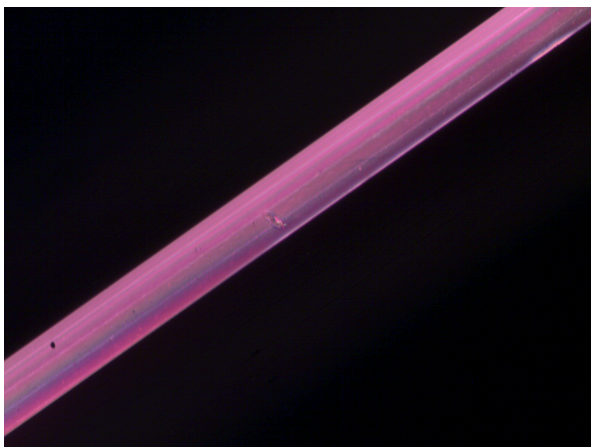


Figure 23: The LC through the polarizer microscope with an external voltage source of 5 V_{RMS} at a frequency of 200Hz



Figure 24: The LC through the polarizer microscope with an external voltage source of 5 V_{RMS} at a frequency of 20kHz

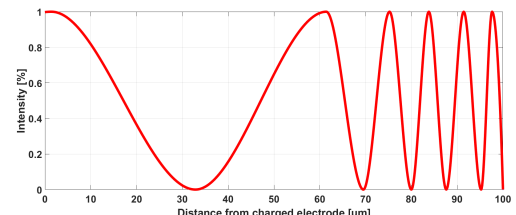


Figure 25: Intensity profile processed from the 5v_{RMS} 200Hz voltage source

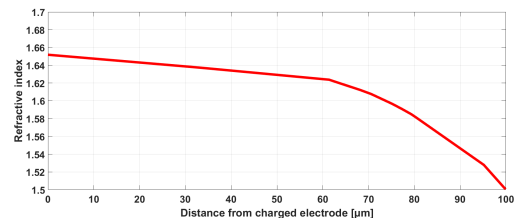


Figure 26: Refractive index profile processed from the 5v_{RMS} 200Hz voltage source

drop seen in Figure 15, the index profile is no longer linear. As regards the optimization, it is highly likely from Table 1 that using a second voltage yields no improvement. Such a conclusion has to be drawn with care as a numerical optimization does not guarantee that a global minimum of the cost function has been found.

5.2. Cross section simulation

The fact that the linear index remains the same at the left electrode for the 1D case (see figure 18) is simply because the average effective index is calculated beforehand as a function of voltage (see figure 7). On the contrary in the 2D case the right electrode also has an influence. At the left electrode the tilt angle would be small (this can be seen from figure 7, the index stays approximately constant up to the threshold voltage of 1 V). But due to the presence of the right electrode at a higher voltage the directors tilt a little more, resulting in a lower refractive index. Over most of the gap the 2D simulation shows a higher refractive index, thus the directors tilt less. This is likely to be due to the use of the one-constant approximation.

5.3. Polarization microscope images

From figures 21 to 25 two things are noticeable, for a higher voltage and lower frequency the interference pattern permeates deeper across the electrodes. As previously shown in figure 14 one would expect the fringes to be equidistant yet this is not the case, this is because a single voltage source was placed on the LC, which does not give a linear change in refractive index. As mentioned earlier, these pictures are only used to check the effects of different voltages and frequencies.

The reason why the interference pattern permeates deeper across the electrodes for a higher voltage is the following, because the voltage difference between both electrodes increases the slope of the voltage across the electrodes, and the voltage drops exponentially across the electrodes, a larger "portion" of the voltage is high enough to cause the LC molecules to change direction due to the electric field, which causes a bigger portion with a varying refractive index. The reason why the interference pattern permeates deeper across the electrodes for a lower frequency can be explained using the following simple model for the LC, in principle the germanium layer and the liquid crystal act as a resistor and capacitor respectively for an AC voltage source. So if the device gets modeled as in figure 27 the total impedance can be calculated. In order to understand

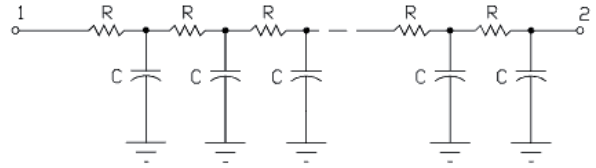


Figure 27: RC circuit equivalent to the germanium layer and LC

why the interference pattern permeates deeper it is sufficient enough to look at the expression for the impedance of a capacitor:

$$Z_C = \omega C = 2\pi f C \quad (45)$$

With f the frequency of the voltage source in hertz and C the capacitance in farads. Now it becomes obvious that for a lower frequency the interference pattern permeates deeper because the capacitor impedance is lower, causing the voltage to drop slower across the electrodes which again causes a bigger portion of the voltage across the electrodes to be big enough to rotate the LC molecules.

6. Experimental results

To check the accuracy of previously discussed theoretical models, experimentation has to be done. An experiment was performed in which the laser was focused between a $100 \mu m$ gap of the beam steering device. In previous sections it was theoretically determined that, in order to get a linearly varying refractive index while still obeying the validity intervals of the theoretical model, the RMS-Voltage on the electrodes should be approximately between 1 and 2 volt. Thus, on one electrode a RMS-voltage of 1 volt was applied while on the other the voltage was varied from 1.0 to 2.5 volt in steps of 0.1 (at a frequency of 5 kHz). The light intensity profiles were measured using a definition camera (BASLER acA2000-165uc) in a darkened room. The RGB images were processed into gray-value intensity profiles using MATLAB, this is displayed in figure 29 and figure 30. By integrating the profiles and using the intensity as weighting, the central position of intensity was determined for each measurement. These positions were then compared to that of the neutral position where the potential difference on the electrodes is zero, clarified in figure 31. The correct scale of the measurements was taken into account by marking dimensions onto the observation plane 32. This way the steering angle can be determined knowing that the observation plane is located 50 cm away from the liquid crystal. In addition, the theoretical steering angles were calculated

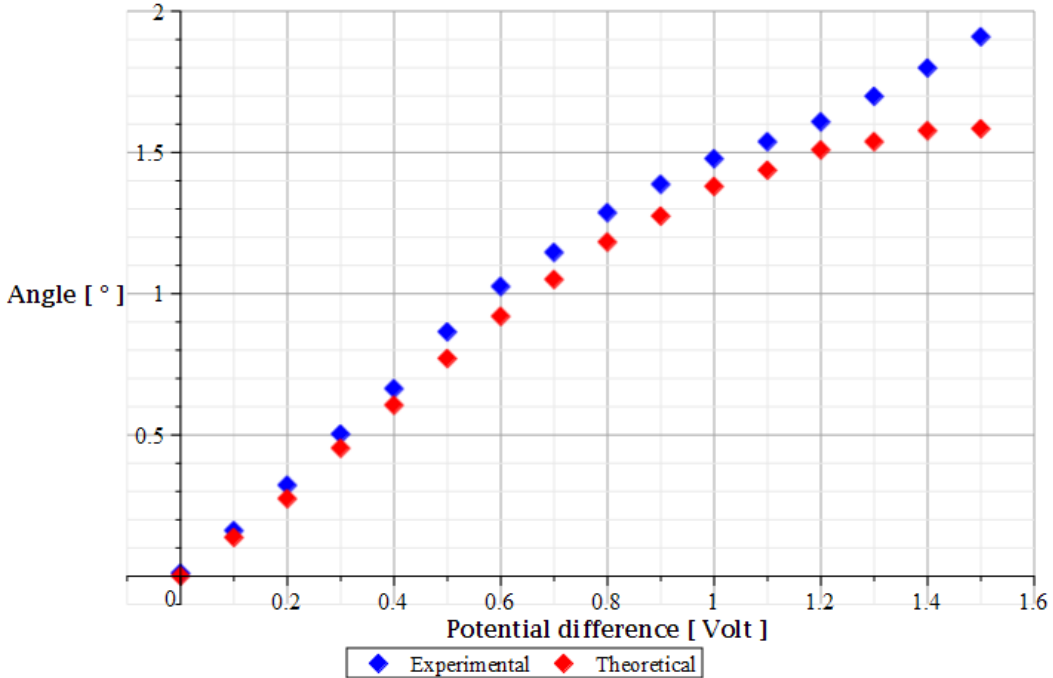


Figure 28: Experimental vs Theoretical results at 1.0-2.5 volt RMS

for the exact same parameters as the performed experiment using the 1D model. Together, these results are graphed in figure 28.

It is clear that at the origin these two should correspond since there is no steering possible when there is no potential difference between the electrodes. As the potential difference gets higher, the theoretical model and experimental measurements still show a very similar trend. The biggest deviations between the two is approximately only 0.1° (10.3%). However, once the variable applied RMS-voltage is significantly higher than 2 volt, the measured intensity profile no longer looks Gaussian and the correlation between theory and observation seems all but lost 33. Note that even the unsteered beam is not very Gaussian, this is a combination of several reasons: impurities of the sample, interference of reflected light within the setup and the beam not being perfectly focused between the gap. Note that focusing the beam too much is also an unwanted property since this would cause the beam to diverge more when leaving the sample. Since the observation plane is located 50 cm away from the LC, this could make the intensity profile unmeasurable.

Although the theoretical model doesn't correctly predict the steering angle in the further region, the theoretically predicted refractive index profile is not linear



Figure 29: Camera images for 1-1 volt RMS (right)

showing that Gaussian beam steering is not possible 34. It is concluded that the approximations made in the 1D model for these parameters don't suffice the used steering device past 2.1 volt RMS.

Although it has now been shown that the theoretical simulation models the beam steering device with reasonable accuracy, its application scope is rather small. That doesn't withhold from exploring other parameters however, that don't nearly fit the requirements to match either of the previous simulations.

In fig 35 beam steering is displayed between a $20\ \mu m$ gap with one of the electrodes grounded while the other has a 5 volt signal with frequency of 50 kHz applied to it. This sample also has a much thinner germanium layer that probably doesn't make contact with the electrodes. However, due to the small gap this becomes

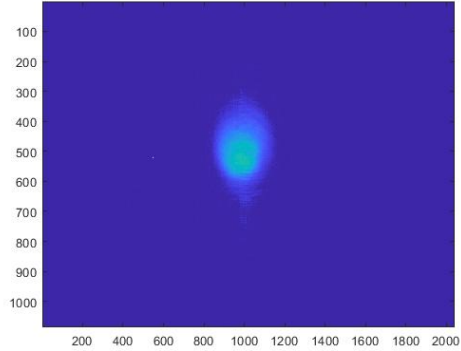


Figure 30: MATLAB gray value color map for 1-1 volt RMS (note: not up to scale, stretched vertically)

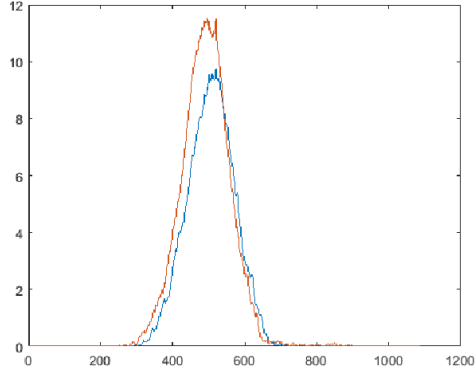


Figure 31: Intensity profile integrated in vertical dimension for 1.2 volt RMS (red) and 1 volt RMS (blue)

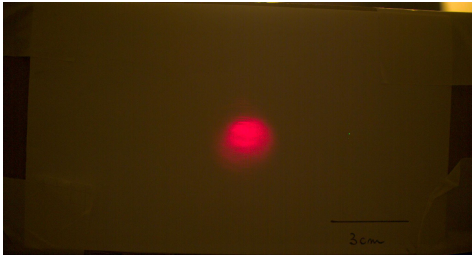


Figure 32: Camera images for 1-1 volt RMS with 3 cm for scaling



Figure 33: smudged intensity profile when variable RMS voltage exceeds 2 volt

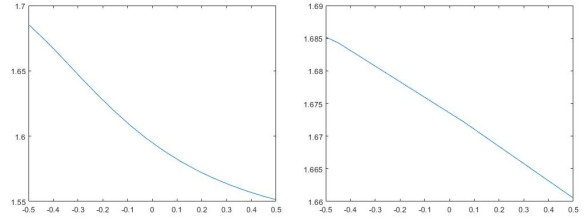


Figure 34: Refractive index profile for 2.5 volt RMS (left, not linear) and 1.2 volt RMS (right, approximately linear)

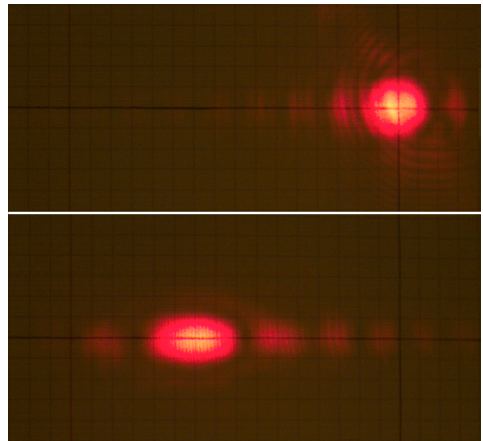


Figure 35: No voltages (top) voltages 0-5 volt at 50 kHz (bottom)

negligible. Despite these unforeseen defect, the beam was steered over an angle of almost 10° while mostly maintaining its shape. In addition, due to the high voltage, the time interval in which this switching takes place is approximately 1 seconds which is significantly faster than the speeds for previous experimental results.

In fig 36 beam steering is displayed for a gap of $50 \mu\text{m}$ in which the phase between the voltages applied to the electrodes is relatively shifted. The RMS voltages on the electrodes are in booth cases 1-3 volt, instead, the joint frequency of the electrode voltages was used as a variable to modulate the steering angle. Note that this doesn't have any influence when the voltages are in phase. The laser beam was steered over approximately 6° .

Booth previous examples don't satisfy the validity interval of the simulations. They also employ degrees of freedom that were not yet made use of and would each add their own new complexity in the differential equations which describe this problem and thus also the complexity of the simulation. This shows that with more advanced modeling techniques and by exploiting other parameters of the problem, the potentials of beam steering could be further investigated in the future.

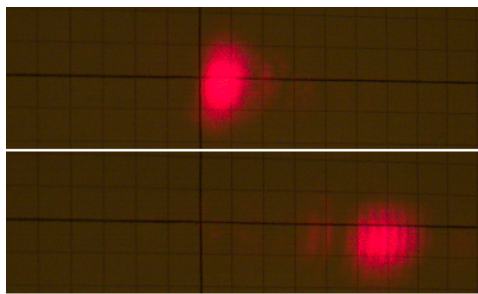


Figure 36: Voltages of 1-3 volt RMS, 1kHz (top), 100Khz (bottom)

7. References

- [1] S. P. Yadav and S. Singh, "Carbon nanotube dispersion in nematic liquid crystals: An overview," *Progress in Materials Science*, vol. 80, pp. 38 – 76, 2016.
- [2] J. Beeckman, I. Nys, O. Willekens, and K. Neyts, "Optimization of liquid crystal devices based on weakly conductive layers for lensing and beam steering," *JOURNAL OF APPLIED PHYSICS*, vol. 121, no. 2, 2017.
- [3] D. Andrienko, "Introduction to liquid crystals," *Journal of Molecular Liquids*, 2018.
- [4] D. Van Thourhout, R. Baets, and H. Ottevaere, *Microphotonics*. 2017.